Influence of Network Voltage Level, Converter Topology and Integration of Energy Storage on the Power Losses of STATCOM Devices

Antti Virtanen, Juha Jokipii, Jenni Rekola and Heikki Tuusa
Tampere University of Technology
Department of Electrical Energy Engineering
Tampere, Finland
Email: antti.a.virtanen@tut.fi

***Abstract*—This paper presents an analysis of power losses in 2.1 MVA static synchronous compensator (STATCOM) devices and STATCOMs with integrated energy storage (ESTATCOM). The analysis was carried out by means of computer simulations, with the main focus on studying the influence of network voltage level (690 V – 2 kV), voltage source converter (VSC) topology (2- or 3-level) and energy storage integration on the losses of STATCOMs. Power loss models for LCL-filters, VSC bridges, DC/DC converter power stages and inductors, as well as supercapacitor banks were developed. According to the results the losses are minimized when a 3-level VSC is used, and the compensator is connected to the network voltage of 690 V, and the ESTATCOM energy storage is connected to the dc link with two separate DC/DC converters. This occurs because the system converters can be implemented with IGBTs of lowest rated voltage.**

I. INTRODUCTION

Nowadays high energy efficiency and low losses are becoming increasingly important in the field of power electronics. This also applies to the design process of power electronic compensators, such as the static synchronous compensators (STATCOM), which are typically used for compensation of e.g. voltage sags, voltage flicker, voltage unbalances and harmonics in power systems [1–5]. The conventional STATCOM is used to regulate the power system voltage by exchanging reactive power with the network. This requires only a small energy storage (ES) in the system dc link. With the integration of a large ES into the device a STATCOM with energy storage (ESTATCOM) is formed, which, in addition to the reactive power exchange, is also capable of exchanging active power with the network. This can be beneficial in cases where power quality problems are caused by the fluctuating active power, especially in weak networks [6], [7].

This paper studies the influence of network voltage level, converter topology and ES integration on the power losses of STATCOM- and ESTATCOM devices, designed for compensation of voltage flicker within electric arc furnaces. The aim was to develop simulation models for the evaluation of power losses in the compensator components – converter bridges and passive elements. In addition the power loss models should be applicable to large-scale system models in the form of a look-up table, to ease the computational burden in long-term simulations. In the paper power losses for a total amount of 18 compensator configurations are studied and a comparison between these is presented. The models were developed with Matlab Simulink software.

Section II presents an overview of the compensator systems studied. Section III presents the operating principles and the theory behind the component power loss models and Section IV presents the comparison of the losses and efficiencies between the different compensator configurations. Finally, conclusions are drawn in Section V.

II. SYSTEMS STUDIED

Fig. 1 presents an overall picture of the studied systems. The conventional STATCOMs consist of a shunt-connected voltage source converter (VSC), an LCL-filter, and the dc link capacitors C_{dc}. The conventional STATCOMs can be upgraded to ESTATCOMs by connecting an ES to the system dc link. The ESs are connected to the dc link with either a single 1.1 MW bidirectional DC/DC converter, or with two parallel 0.55 MW converters in which two separate ES units are connected over the upper and lower dc link capacitors as presented with the dashed line in Fig. 1.

The rated power of the compensator VSCs is 2.1 MVA and the compensators were studied with grid line-to-line voltages of 2 kV, 1 kV and 690 V. The respective dc link voltages were 3500 V, 1750 V and 1200 V and the energy storage maximum voltages 2500 V, 1250 V and 875 V with the single 1.1 MW DC/DC converters, and 1250 V, 625 V and 500 V with the two parallel 0.55 MW converter configurations.

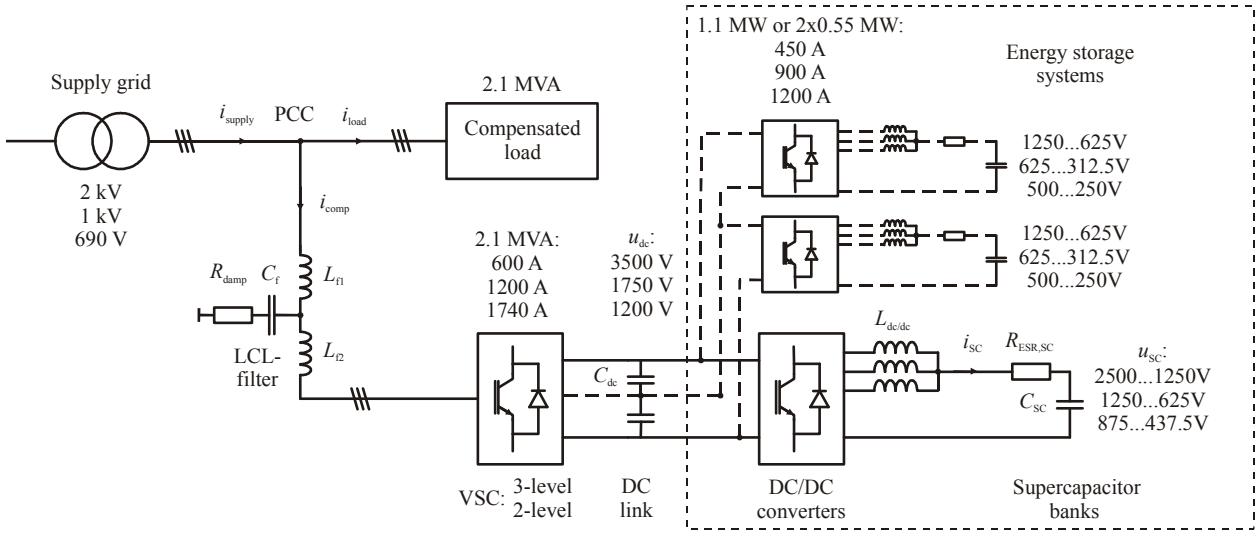

Figure 1. Overall picture of the studied systems.

The VSC bridge topologies in the analysis are either 2-level converters or 3-level neutral point clamped (NPC) converters, which in all cases use sine-triangle PWM with 3rd harmonic injection with the switching frequency of f_{sw} = 4 kHz [8,9]. The DC/DC converters are 3-phase step-up/step-down converters with 120° interleaved PWM modulation with f_{sw} = 4 kHz [10]. The ESs are supercapacitor (SC) banks built-up of case-specific series- and parallel connections of Maxwell BMOD0063 P125 modules for maximum continuous total power of 1.1 MW, with maximum continuous current of 150 A for a single module [11]. Table I presents the SC configurations of the systems studied.

Table II presents the passive elements of the systems studied. Each LCL-filter was designed for maximum compensator current i_{comp} THD of 2 %, and for maximum $i_{comp,rms}$ switching frequency ripple of 2 %. The resonance frequency of each filter is 1620 Hz. The DC/DC converter inductors $L_{dc/dc}$ were designed for a maximum peak-to-peak current ripple of 10 % in the SC current i_{SC}. The SC bank capacitances C_{SC} and the equivalent series resistances $R_{ESR,SC}$ were calculated on the basis of single module parameters C_{SC} = 63 F and $R_{ESR,SC}$ = 18 mΩ, found in the manufacturer's datasheet and [11].

III. Simulation Models of Component Power Losses

This section presents the operating principles and theory behind the simulation models used for calculating the component power losses. Separate models were developed for the LCL-filters, VSC bridges and DC/DC converter power stages, DC/DC converter inductors and the SC banks. Each component model is applicable to large-scale system models in the form of a look-up table in order to ease the computational burden during future long-term simulations.

A. LCL-filter Power Loss Model

The LCL-filter power loss model takes into account the hysteresis and eddy current losses in the core, and the resistive

TABLE I. SUPERCAPACITOR BANKS OF THE STUDIED SYSTEMS

System	Modules in series	Series connections in parallel
1.1 MW 2 kV	20	3
2×0.55 MW 2 kV	10	3×2
1.1 MW 1 kV	10	6
2×0.55 MW 1 kV	5	6×2
1.1 MW 690 V	7	8
2×0.55 MW 690 V	4	8×2

TABLE II. COMPONENTS OF THE SYSTEMS STUDIED

System	L_{f1} [mH (p.u.)]	L_{f2} [mH (p.u.)]	C_f [mF (p.u.)]	R_{damp} [Ω (p.u.)]	C_{dc} [mF (p.u.)]	$L_{dc/dc}$ [mH (p.u.)]	C_{SC} [F (p.u.)]	$R_{ESR,SC}$ [mΩ (p.u.)]
3-Level 2kV / 2×DCDC	0.1 (0.016)	0.4 (0.063)	0.12 (0.075)	1.33 (0.67)	4.8 (3.0)	1.6 (0.25) / 2×0.8 (0.125)	9.45 (5900) / 2×18.9 (11800)	120 (0.06) / 2×60 (0.03)
3-Level 1kV / 2×DCDC	0.025 (0.016)	0.1 (0.063)	0.48 (0.075)	0.33 (0.67)	19.2 (3.0)	0.4 (0.25) / 2×0.2 (0.125)	37.8 (5900) / 2×75.6 (11800)	30 (0.06) / 2×15 (0.03)
3-Level 690V / 2×DCDC	0.0125 (0.017)	0.05 (0.066)	0.96 (0.072)	0.17 (0.70)	40.3 (3.0)	0.21 (0.27) / 2×0.105 (0.135)	72.0 (5360) / 2×126 (9380)	16 (0.07) / 2×9 (0.04)
2-Level 2kV / 2×DCDC	0.2 (0.032)	0.8 (0.126)	0.06 (0.037)	2.66 (1.33)	4.8 (3.0)	1.6 (0.25) / 2×0.8 (0.125)	9.45 (5900) / 2×18.9 (11800)	120 (0.06) / 2×60 (0.03)
2-Level 1kV/ 2×DCDC	0.05 (0.032)	0.2 (0.126)	0.24 (0.037)	0.67 (1.33)	19.2 (3.0)	0.4 (0.25) / 2×0.2 (0.125)	37.8 (5900) / 2×75.6 (11800)	30 (0.06) / 2×15 (0.03)
2-Level 690V / 2×DCDC	0.025 (0.033)	0.1 (0.132)	0.48 (0.036)	0.33 (1.4)	40.3 (3.0)	0.21 (0.27) / 2×0.105 (0.135)	72.0 (5360) / 2×126 (9380)	16 (0.07) / 2×9 (0.04)

and eddy current losses in the winding conductors for inductors L_{f1} and L_{f2} [12]. The analysis is performed at the fundamental 50 Hz frequency, and around the switching frequency and its 2nd multiple (i.e. 4 kHz and 8 kHz). In addition the fundamental frequency losses in the LCL-filter damping resistors R_{damp} were included in the analysis. The losses in the filter capacitors C_f are insignificant compared to the inductor losses, and are hence ignored.

The parameters needed in the calculations are the core type, core material, core cross-sectional area A_{core}, winding material, core mass m_{core}, airgap length l_{ag}, number of winding turns N, winding wire length l_{wire}, wire cross-sectional area A_{wire}, wire thickness h_{wire}, and the number of winding layers M. Table III presents these parameters for the both filter inductors in the 3-Level 2 kV system, which is used as an example in the following calculations.

The inductances per-phase for all systems (Table II) are calculated from

$$L = \frac{1.11 \cdot \mu_0 \cdot A_{core} \cdot N^2}{l_{ag}}, \quad (1)$$

where $1.11 \cdot \mu_0 = 1.11 \cdot 4 \cdot \pi \cdot 10^{-7}$ H/m is the permeability of the airgap medium. In all the systems the core dimensions A_{core} and m_{core} were assumed to be equal to the values presented in Table III. The inductances for the other 3-level systems are found by reducing N with the ratio of the system voltage levels (i.e. 1 kV/2 kV or 690 V/2 kV). At the same time l_{wire} is reduced with the same ratio, but A_{wire} is increased because the nominal current in the lower voltage systems increases. The inductances in the 2-level systems are found by doubling N and l_{ag} in comparison to the corresponding 3-level systems. At the same time l_{wire} is doubled, which also doubles the number of winding layers.

The LCL-filter power loss modeling process begins by first determining the high frequency ripple components in the L_{f1} current (i_{comp} in Fig. 1). Figs. 2a,b present the waveform and the normalized amplitude spectrum of i_{comp} within the nominal operating point of 2.1 MVA. The RMS value of the fundamental frequency component is $I_{rms,50Hz} = 637$ A (901 A/√2 in Fig. 2b), and the respective harmonic components around the switching frequency and its 2nd multiple are $I_{rms,4kHz} = 6.6$ A (1.1 %) and $I_{rms,8kHz} = 3.9$ A (0.65 %). The LCL-filter design constraints are satisfied, since the THD is 1.4 % and the switching frequency harmonic components are below 2 %.

1) Fundamental Frequency Core Losses

The fundamental frequency core losses are mainly caused by the hysteresis phenomenon in the inductor core [12]. These can be determined on the basis of the core material and weight, and the characteristic core loss curve for the M470-50A laminated iron. The core loss curve is provided by the manufacturer of the electrical steel, and is presented in Fig. 2c. The curve displays the core losses at 50 Hz in [W/kg] as a function of the core magnetic flux density

TABLE III. PARAMETERS OF THE LCL-FILTER INDUCTORS IN THE 3-LEVEL 2 KV SYSTEM

Parameter	Inductor L_{f1}	Inductor L_{f2}
Core type	3-phase EI	3-phase EI
Core material	Non-oriented M470-50A	Oriented M6
Core area, A_{core}	85 cm^2	110 cm^2
Winding material	Aluminium	Aluminium
Core mass, m_{core}	117.7 kg	249.1 kg
Airgap length, l_{ag}	14 mm	27 mm
Number of turns, N	11	26.5
Wire length, l_{wire}	5.65 m	15.65 m
Wire area, A_{wire}	500 mm^2	520 mm^2
Wire thickness, h_{wire}	22.4 mm	22.8 mm
Number of winding layers, M	1	1

$$B = \frac{1.11 \cdot \mu_0 \cdot N \cdot \sqrt{2} \cdot I}{l_{ag}}. \quad (2)$$

The losses are found by calculating the magnetic flux density with different current values, and by comparing the calculated flux densities with the characteristic loss curve. The obtained losses are then multiplied by the core weight and can be calculated as a function of the inductor current, as presented in Fig. 2d. With 637 A the 50 Hz core losses are 224 W.

2) Fundamental Frequency Winding Losses

The winding losses at the fundamental frequency are caused by the current flowing through a wire with electrical resistance [12]. These are obtained by first calculating the resistance of the wire in each phase

$$R_{wire,50Hz} = \frac{\rho_{Al} \cdot l_{wire}}{A_{wire}}, \quad (3)$$

where $\rho_{Al} = 2.655 \cdot 10^{-8}$ Ωm is the resistivity of aluminium. After calculation of $R_{wire,50Hz}$ the 3-phase fundamental frequency winding losses are obtained from

$$P_{wind,50Hz} = 3 \cdot R_{wire,50Hz} \cdot I^2_{rms,50Hz}, \quad (4)$$

and presented in Fig. 2d. With 637 A the winding losses are 365 W.

3) High Frequency Core Losses

High frequency (HF) core losses are mainly caused by the HF eddy currents induced into the core material [12]. These can be determined on the basis of the HF core loss curves, provided by electrical steel manufacturers. Fig. 2e presents the HF core loss curves for M470-50A electrical steel with the respective frequencies of 2 kHz, 4 kHz, 5 kHz, 8 kHz and 10 kHz as a function of the magnetic flux density. The HF core losses are found by first calculating the magnetic flux densities generated by the ripple currents at 4 kHz and 8 kHz from (2). After this the HF core losses can be calculated as a function of the ripple current, in the same manner as for the fundamental frequency core losses. The HF core losses are presented in Fig. 2f as a function of the inductor ripple current. The HF core losses are 60 W around the switching frequency

of 4 kHz (with $I_{\mathrm{rms,4kHz}} = 6.6$ A), and 88 W around the 2nd multiple of the switching frequency 8 kHz (with $I_{\mathrm{rms,8kHz}} = 3.9$ A).

4) High Frequency Winding Losses

The HF winding losses are caused by the skin effect and proximity effect mechanisms [12]. The skin effect increases the current density in a wire exponentially as a function of frequency. This leads to reduction of the wire effective cross-sectional area, and hence increased R_{wire} especially with high frequencies. The proximity effect increases the eddy currents, and hence the winding losses, within closely wound inductor wires, especially at high frequencies.

To model the combined effect of these mechanisms the skin depth δ is first calculated [12]

$$\delta = \sqrt{\frac{\rho_{\mathrm{Al}}}{\pi \cdot \mu_0 \cdot f}}, \tag{5}$$

where the frequency f is expressed in Hz. Next the factor φ is calculated from

$$\varphi = \frac{h_{\mathrm{wire}}}{\delta}, \tag{6}$$

where h_{wire} is the wire thickness. The resistance of the inductor wire experienced at HF $R_{\mathrm{wire,HF}}$ is found from

$$R_{\mathrm{wire,HF}} = F_{\mathrm{R}} \cdot R_{\mathrm{wire,50Hz}}, \tag{7}$$

where

$$F_{\mathrm{R}} = \varphi\left[G_1(\varphi) + \frac{2}{3}(M^2 - 1)(G_1(\varphi) - 2G_2(\varphi)) \right], \tag{8}$$

and functions $G_1(\varphi)$ and $G_2(\varphi)$ are

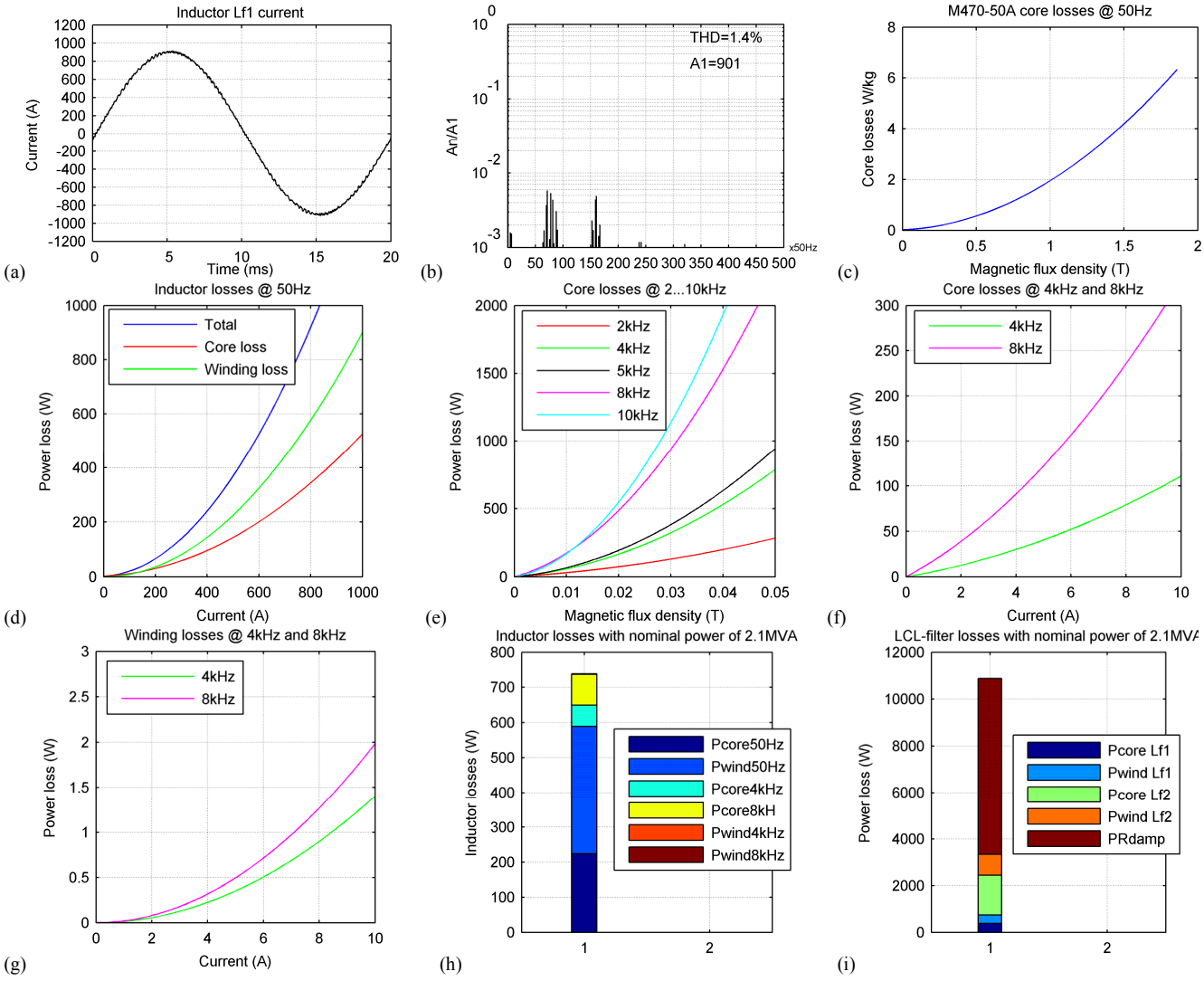

Figure 2. Power loss modelling of inductor L_{f1} in the 3-level 2 kV system. (a) Inductor current, (b) normalized amplitude spectrum of inductor current, (c) characteristic core loss curve for M470-50A electrical steel, (d) inductor core- and winding losses at 50 Hz, (e) high frequency core loss curves for M470-50A electrical steel, (f) high frequency core losses, (g) high frequency winding losses, (h) inductor total losses, (i) LCL-filter total losses.

$$G_1(\varphi) = \frac{\sinh(2\varphi) + \sin(2\varphi)}{\cosh(2\varphi) - \cos(2\varphi)}, \quad (9)$$

$$G_2(\varphi) = \frac{\sinh(\varphi)\cos(\varphi) + \cosh(\varphi)\sin(\varphi)}{\cosh(2\varphi) - \cos(2\varphi)}, \quad (10)$$

and M is the number of winding layers.

The HF winding losses are finally calculated from

$$P_{\text{wind,HF}} = 3 \cdot R_{\text{wire,HF}} \cdot I^2_{\text{rms,4\&8kHz}}, \quad (11)$$

and presented in Fig. 2g. For the inductor L_{f1} these losses are negligible, below 1 W for both 4 kHz and 8 kHz ripple currents. However, multiple layer windings and greater current ripple may dramatically increase the HF winding losses [12].

5) LCL-filter Total Losses

Fig. 2h presents a bar graph of the total losses for the 3-level 2 kV system inductor L_{f1}. The 50 Hz winding- and core losses are the most dominant, while the HF core losses are relatively small because of the small ripple component of i_{comp}. The HF winding losses are insignificant to the result. Fig. 3i presents a bar graph of the LCL-filter total losses including also the losses of L_{f2} and the fundamental frequency losses in R_{damp} for the 3-level 2 kV system. The losses of L_{f2} were obtained with the same procedure as presented for L_{f1}, and the losses in R_{damp} were determined from

$$P_{\text{loss,Rdamp}} = 3 \cdot R_{\text{damp}} \cdot \left(\frac{(U_{\text{LL}} / \sqrt{3})}{\sqrt{1/(\omega_{\text{grid}} \cdot C_{\text{f}})^2 + R^2_{\text{damp}}}} \right)^2. \quad (12)$$

In this case approximately 2/3 of the losses arise in the LCL-filter damping resistors.

Fig. 3 presents the LCL-filter losses for all systems studied. The 3-level systems total losses are slightly higher than the 2-level system losses because of the higher power loss in the R_{damp}. The loss distribution in the 3-level system inductors differs slightly from the 2-level system. In the 3-level system inductors the core losses are dominant, but in the 2-level inductors the highest losses appear in the windings.

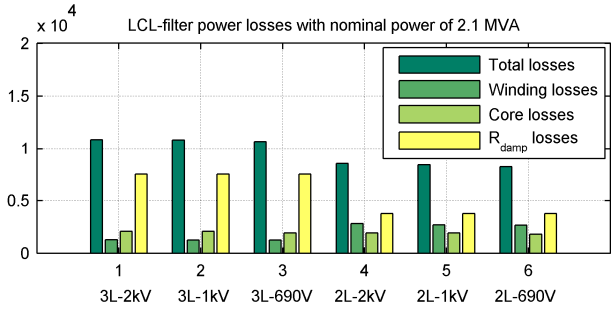

Figure 3. LCL-filter power losses with nominal power.

This is due to the increased wire length and the increased amount of winding layers in the 2-level inductors compared to the 3-level inductors.

B. VSC Bridge and DC/DC Converter Power Stage Power Loss Models

The power loss models of the VSC bridges and DC/DC converter power stages calculate the conduction - and switching losses of the IGBTs and diodes as a function of the instantaneous IGBT - and diode currents. The simulation model recognizes every switching - and conduction occasion for each power electronic switching device. The calculated losses for the single switching and conduction instants are then summed and averaged over the fundamental time period of $T = 20$ ms.

The IGBT-modules used in the VSC bridges and DC/DC converter power stages are presented in Table IV, which shows that the converters connected to grid voltages of 1 kV and 690 V can be implemented with IGBTs of lower rated voltage (V_{CE}) than those connected to the 2 kV supply. The same behavior can be seen when the IGBTs of the 3- and 2-level VSCs, as well as the IGBTs of the single and double DC/DC converter configurations are compared. However, in order to satisfy the required current rating, several 1200 A IGBTs are needed in parallel within the 1 kV and 690 V VSCs, and naturally the use of two parallel DC/DC converters doubles the amount of switching devices.

1) Conduction Losses

The average conduction losses of the IGBTs and diodes in the converter bridges are calculated according to the following

TABLE IV. IGBT COMPONENTS OF VSC BRIDGES AND DC/DC CONVERTER POWER STAGES

System	VSC IGBTs		DC/DC Converter IGBTs	
3-Level 2kV / 2×DCDC	ABB 5SNA1200E330100	V_{CE} = 3300 V I_C = 1200 A	ABB 5SNA0400J650100 / 2×Infineon FZ400R33KL2C B5	V_{CE} = 6500 V, I_C = 400 A / V_{CE} = 3300 V, I_C = 400 A
3-Level 1kV / 2×DCDC	2×Infineon FZ1200R17HP4	V_{CE} = 1700 V I_C = 1200 A	ABB 5SNA0800N330100 / 2×Infineon FZ800R17KF6C B2	V_{CE} = 3300 V, I_C = 800 A / V_{CE} = 1700 V, I_C = 800 A
3-Level 690V / 2×DCDC	3×Infineon FZ1200R12HP4	V_{CE} = 1200 V I_C = 1200 A	ABB 5SNA1200E250100 / 2×Infineon FZ1200R12HP4	V_{CE} = 2500 V, I_C = 1200 A / V_{CE} = 1200 V, I_C = 1200 A
2-Level 2kV / 2×DCDC	ABB 5SNA1200G450350	V_{CE} = 4500 V I_C = 1200 A	ABB 5SNA0400J650100 / 2×Infineon FZ400R33KL2C B5	V_{CE} = 6500 V, I_C = 400 A / V_{CE} = 3300 V, I_C = 400 A
2-Level 1kV / 2×DCDC	2×ABB 5SNA1200E330100	V_{CE} = 3300 V I_C = 1200 A	ABB 5SNA0800N330100 / 2×Infineon FZ800R17KF6C B2	V_{CE} = 3300 V, I_C = 800 A / V_{CE} = 1700 V, I_C = 800 A
2-Level 690V / 2×DCDC	3×ABB 5SNA1200E250100	V_{CE} = 2500 V I_C = 1200 A	ABB 5SNA1200E250100 / 2×Infineon FZ1200R12HP4	V_{CE} = 2500 V, I_C = 1200 A / V_{CE} = 1200 V, I_C = 1200 A

equations

$$P_{\text{cond,igbt}} = \frac{1}{T}\int_0^T \left(i_{\text{igbt}} \cdot R_{\text{ce}} + V_{\text{t}}\right) \cdot i_{\text{igbt}}\, dt, \tag{13}$$

$$P_{\text{cond,diode}} = \frac{1}{T}\int_0^T \left(i_{\text{diode}} \cdot R_{\text{f}} + V_{\text{f}}\right) \cdot i_{\text{diode}}\, dt, \tag{14}$$

where R_{ce} and R_{f} are the respective on-state resistances, and V_{t} and V_{f} the respective zero-current voltage drops of the IGBTs and diodes. These parameters are found in the manufacturer's datasheets.

2) Switching Losses

The VSC and DC/DC converter switching losses are modeled by determining the turn-on and turn-off energies of the IGBTs, as well as the reverse recovery energies of the diodes within each switching occasion. On average the switching losses are calculated from the following equations

$$P_{\text{igbt,on}} = \frac{1}{T}\sum \frac{u_{\text{dc}}}{u_{\text{cc}}} E_{\text{on}}(i_{\text{igbt}}), \tag{15}$$

$$P_{\text{igbt,off}} = \frac{1}{T}\sum \frac{u_{\text{dc}}}{u_{\text{cc}}} E_{\text{off}}(i_{\text{igbt}}), \tag{16}$$

$$P_{\text{diode,rr}} = \frac{1}{T}\sum \frac{u_{\text{dc}}}{u_{\text{cc}}} E_{\text{rr}}(i_{\text{diode}}), \tag{17}$$

where u_{dc} is the dc link voltage. The parameter u_{cc} is the collector-emitter supply voltage, and $E_{\text{on}}(i_{\text{igbt}})$, $E_{\text{off}}(i_{\text{igbt}})$, and $E_{\text{rr}}(i_{\text{diode}})$ are the switching component turn-on, turn-off, and reverse recovery energies as a function of collector-emitter current. These parameters are all found in the manufacturer's datasheets.

3) VSC Bridge and DC/DC Converter Power Stage Power Losses in Nominal Operating Point

Figs. 4a,b present the power losses for all VSC and DC/DC converter power stage configurations studied with VSC nominal power of 2.1 MVA, and DC/DC converter nominal power of 1.1 MW. The lowering of the network voltage from 2 kV to 1 kV or 690 V significantly reduces the power losses in both converters. This is mainly due to the use of the IGBTs with lower rated voltage in the converter bridges (Table IV), which produce significantly lower switching losses than those with the higher voltage rating. The same reason causes the systems with the 3-level VSCs to produce lower losses than the systems with 2-level VSCs. In addition a similar trend can be noticed when two separate DC/DC converters are used instead of a single converter unit.

C. DC/DC Converter Inductor Power Loss Models

The power loss model of the DC/DC converter inductors $L_{\text{dc/dc}}$ takes into account the core hysteresis and eddy current losses as well as the resistive and eddy current losses in the inductor windings at dc frequency, and around the switching frequency and its 2nd multiple (i.e. 4 kHz and 8 kHz) [12]. The

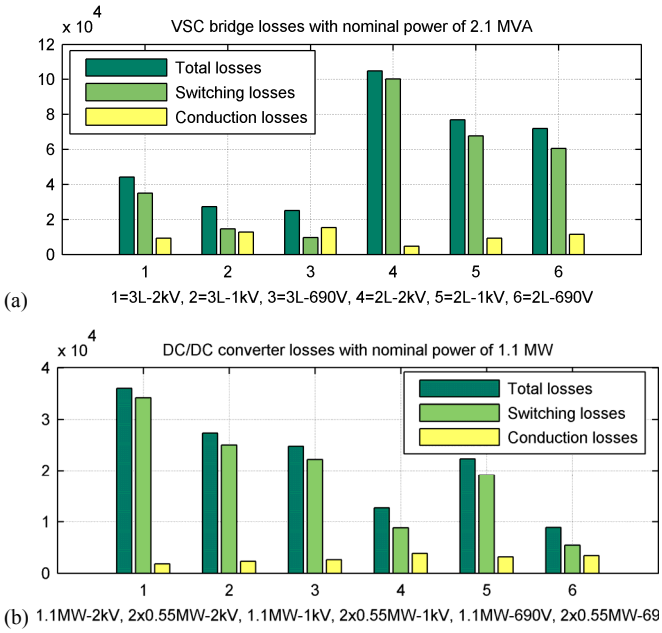

Figure 4. Power losses with nominal power for the (a) VSC bridges, (b) DC/DC converter power stages.

modeling procedure is similar to the LCL-filter inductors, presented in Section III.A.

Table V presents the parameters for the DC/DC converter inductors in the single 1.1 MW and for the double 0.55 MW configurations at the 2 kV grid voltage. The inductances of the other DC/DC converter configurations (Table II) can be calculated from (1) by reducing N with the ratio of the system voltage levels (i.e. 1 kV/2 kV or 690 V/2 kV). At the same time l_{wire} is reduced with the same ratio, but A_{wire} is increased since the nominal current increases.

Fig. 5a presents the waveforms of the inductor phase currents and the resulting total current i_{SC} (Fig. 1) for the single DC/DC converter configuration within its nominal operating point of 1.1 MW with u_{dc} = 3500 V and u_{SC} = 2400 V. The peak-to-peak current ripple of i_{SC} is 10 A (2.2 %), which satisfies the design constraints presented in Section II. The normalized amplitude spectrum for the single inductor current is presented in Fig. 5b. The single

TABLE V. PARAMETERS OF THE DC/DC CONVERTER INDUCTORS IN THE 2 KV SYSTEM

Parameter	1.1 MW Inductors	0.55 MW Inductors
Core type	Single phase UI	Single phase UI
Core material	Oriented M6	Oriented M6
Core area, A_{core}	110 cm^2	55 cm^2
Winding material	Aluminium	Aluminium
Core mass, m_{core}	87.5 kg	43.75 kg
Airgap length, l_{ag}	18 mm	18 mm
Number of turns, N	43.5	43.5
Wire length, l_{wire}	23.9 m	17.4 m
Wire area, A_{wire}	135 mm^2	135 mm^2
Wire thickness, h_{wire}	11.6 mm	11.6 mm
Number of winding layers, M	2	2

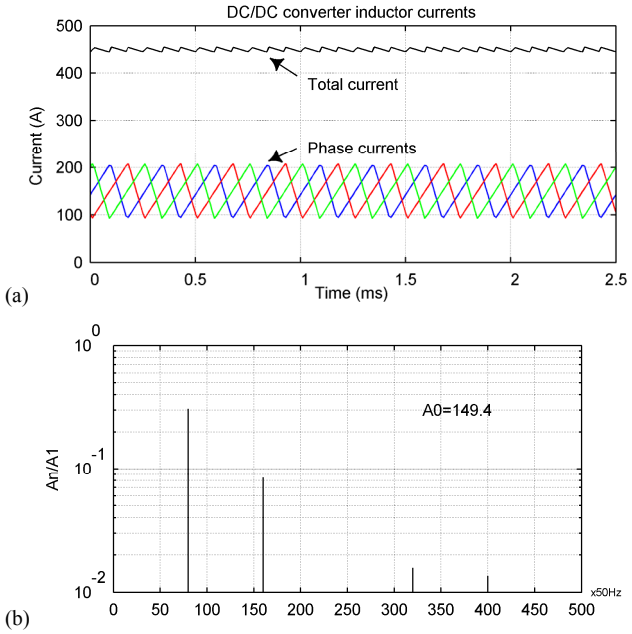

Figure 5. Currents of the single 1.1 MW DC/DC converter inductors with nominal power. (a) Inductor phase currents and total current, (b) normalized amplitude spectrum of inductor phase-A current.

inductor current ripples needed in the power loss modeling procedure are $I_{\text{rms,4kHz}} = 32.5$ A and $I_{\text{rms,8kHz}} = 8.9$ A.

Fig. 6 presents the power losses of all DC/DC converter inductors studied with the nominal power of 1.1MW. The majority of losses occur at the inductor cores, because of the fairly high switching frequency current ripples. No big differences can be seen in the losses between different system configurations.

D. Supercapacitor Bank Losses

The SC bank losses are modeled on the basis of the $R_{\text{ESR,SC}}$ presented in Table II. The SC power losses are calculated from

$$P_{\text{loss,SC}} = R_{\text{ESR,SC}} \cdot i_{\text{SC}}^2 \,. \tag{18}$$

For all of the studied SC bank configurations the power losses with the nominal power of 1.1 MW are $P_{\text{loss,SC}} = 24.3$ kW.

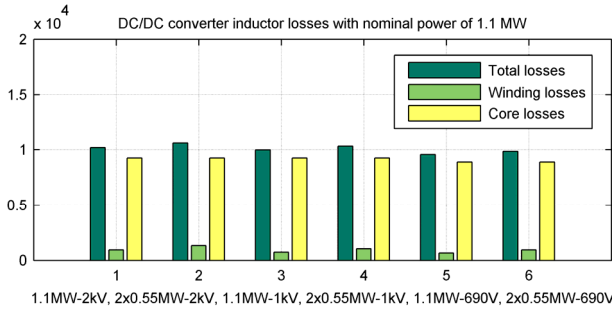

Figure 6. DC/DC converter inductor losses with nominal power of 1.1 MW.

IV. Total Power Losses and Efficiencies of the Compensator Configurations Studied

On the basis of the power loss models and calculations presented in Section III, the total power losses and efficiencies of the STATCOM and ESTATCOM configurations studied are analyzed. The analysis is done with the power levels of 25 % to 100 %, defined respectively in Table VI. Figs. 7a,b present the loss distribution in the components of the compensator configurations with power levels of 100 % and 50 %. Fig. 7c presents the efficiencies of the ESTATCOMs with full and partial loads.

The lowering of the network voltage from 2 kV to 1 kV or 690 V reduces the total losses in all the systems. This is expected since the lower network voltage enables the use of IGBTs with lower rated voltage within the system converters, as discussed in Section III.B.3. The lower voltage IGBTs also produce lower losses when the systems with the 3-level VSCs and double DC/DC converter units are compared with the 2-level VSC and single DC/DC converter systems. The SC bank integration roughly doubles the losses of the ESTATCOMs compared to the conventional STATCOMs. Overall, the lowest losses and the best efficiency are achieved with the system using the 3-level VSC connected to the 690 V network, and when the two parallel 0.55 MW DC/DC converters are used instead of the single 1.1 MW converter.

V. Conclusion

A comparison of power losses between 18 STATCOM and ESTATCOM configurations was presented. Loss models for the LCL-filter, 2- and 3-level VSC bridges, DC/DC converter power stages and inductors, as well as SC banks were developed with Matlab Simulink. Each component power loss model is applicable to large-scale simulation environments in the form of a look-up table. The lowest losses and the best efficiency were achieved with systems using 3-level VSCs connected to the network voltage of 690 V, because these systems can be implemented with IGBTs of the lowest rated voltage. In addition the use of two separate DC/DC converters in the connection of the SC banks to the dc link in ESTATCOM systems is somewhat more energy efficient than using a single converter.

Table VI. Definition of Power Levels in the Compensator Loss Analysis

	ESTATCOM			STATCOM
Power level	**S [MVA]**	**P [MW]**	**Q [MVAr]**	**Q [MVAr]**
100 %	2.1	1.1	1.8	2.1
75 %	1.58	0.825	1.35	1.58
50 %	1.05	0.55	0.9	1.05
25 %	0.525	0.275	0.45	0.525

References

[1] P. Wang, N. Jenkins, M. H. J. Bollen, "Experimental investigation of voltage sag mitigation by an advanced static VAr compensator," *IEEE Transactions on Power Delivery*, vol. 13, no. 4, pp. 1461-1467, Oct. 1998.

[2] M. Routimo, A. Mäkinen, M. Salo, R. Seesvuori, J. Kiviranta, H. Tuusa, "Flicker mitigation with a hybrid compensator," *IEEE*

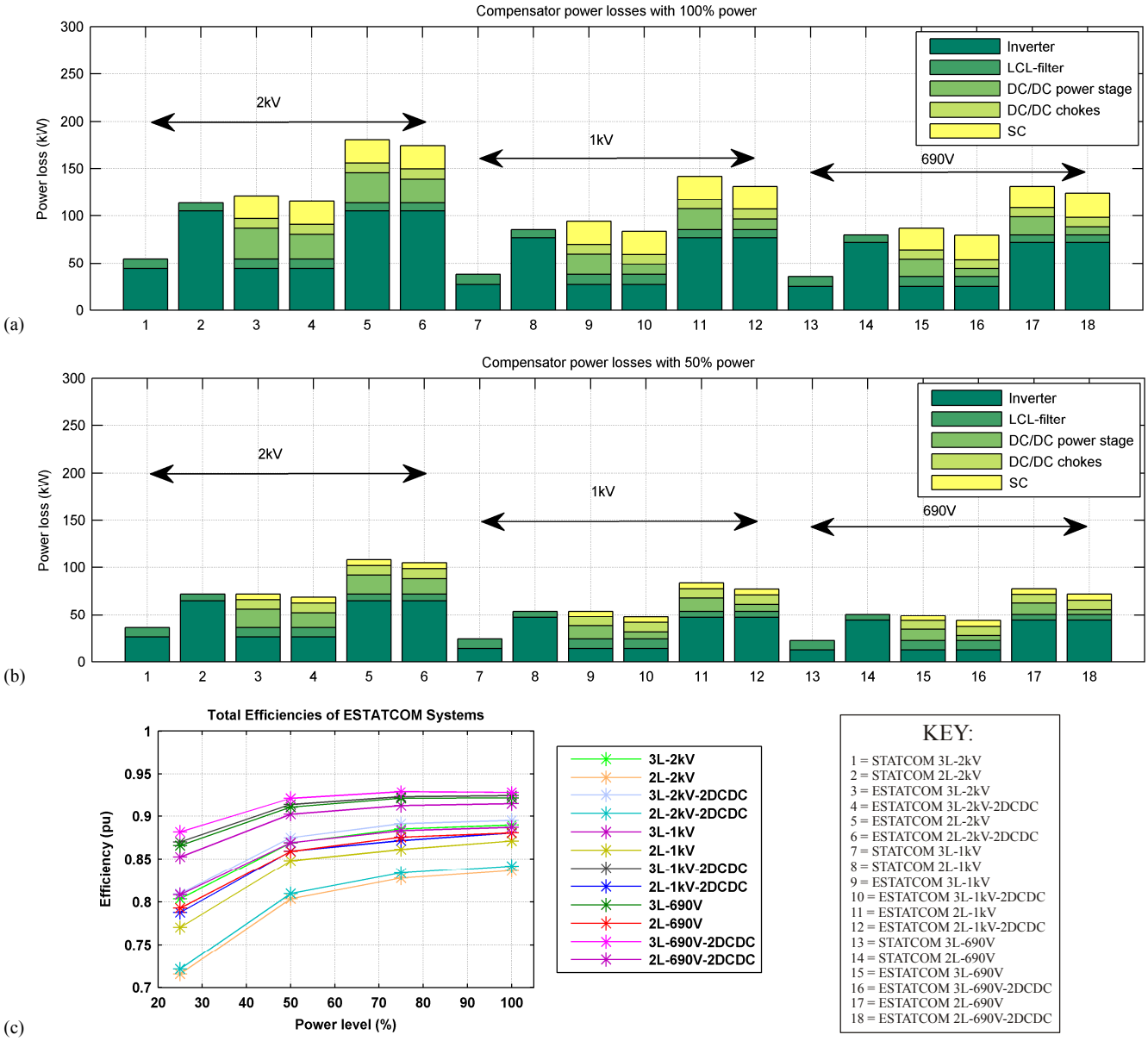

Figure 7. System losses with (a) 100% power, (b) 50% power, and (c) ESTATCOM total efficiencies with power levels of 25 % to 100 %.

Transactions on Industry Applications, vol. 44, no. 4, pp. 1227-1238, Jul./Aug. 2008.

[3] G.F. Reed, M. Takeda, F. Ojima, A. P. Sidell, R. E. Chervus, C. K. Nebecker, "Application of a 5 MVA, 4.16 kV D-STATCOM system for voltage flicker compensation at Seattle Iron and Metals," in *IEEE 2000 Power Engineering Society Summer Meeting*, 2000, vol. 3, pp. 1605-1611.

[4] J. Sun, D. Czarkowski, Z. Zabar, "Voltage flicker mitigation using PWM-based distribution STATCOM," in *IEEE 2002 Power Engineering Society Summer Meeting*, 2002, vol. 1, pp. 616-621.

[5] Y. Xu, L. M. Tolbert, J. D. Kueck, D. T. Rizy, "Voltage and current unbalance compensation using a static var compensator," *IET Power Electronics*, vol. 3, no. 6, pp. 977-988, Nov. 2010.

[6] A. Arulampalam, J. B. Ekanayake, N. Jenkins, "Application study of a STATCOM with energy storage," *IEE Proceedings: Generation, Transmission and Distribution*, vol. 150, no. 3, pp. 373-384, May 2003.

[7] H. Xie, L. Ängquist, H.-P. Nee, "Investigation of StatComs with capacitive energy storage for reduction of voltage phase jumps in weak networks," *IEEE Transactions on Power Systems*, vol. 24, no. 1, pp. 217-225, Feb. 2009.

[8] D. G. Holmes, T. A. Lipo, *Pulse width modulation for power converters: principles and practice*, IEEE Press, Piscataway, New Jersey, USA, 2003, 724 p.

[9] A. Nabae, I. Takahashi, H. Akagi, "A new neutral-point-clamped PWM inverter," *IEEE Transactions on Industry Applications*, vol. IA-17, no. 5, pp. 518-523, Sept./Oct. 1981.

[10] J. Zhang, J.-S. Lai, R.-Y. Kim, W. Yu, "High-power density design of a soft-switching high-power bidirectional dc–dc converter," *IEEE Transactions on Power Electronics*, vol. 22, no. 4, pp. 1145-1153, Jul. 2007.

[11] A. Virtanen, H. Haapala, S. Hännikäinen, T. Muhonen, H. Tuusa, "Calorimetric efficiency measurements of supercapacitors and lithium-ion batteries," in *IEEE 2011 Applied Power Electronics Conference*, 2011, pp. 1367-1373.

[12] R. W. Erickson, D. Maksimovic, *Fundamentals of power electronics*, Kluwer academic publishers, Norwell, Massachusetts, USA, 2001, 883 p.